Chemical Science

View Online
Dynamic Article Links

Cite this: *Chem. Sci.*, 2011, **2**, 1090

www.rsc.org/chemicalscience

EDGE ARTICLE

Kinetics-driven high power Li-ion battery with *a*-Si/NiSi$_x$ core-shell nanowire anodes†

Kibum Kang,[a] Kyeongse Song,[c] Hoseok Heo,[b] Sunyoung Yoo,[a] Gil-Sung Kim,[a] Geunhee Lee,[a] Yong-Mook Kang*[c] and Moon-Ho Jo*[ab]

Received 14th December 2010, Accepted 16th March 2011
DOI: 10.1039/c0sc00628a

We report amorphous-Si nanowire shell anodes, supported by NiSi$_x$ nanowire cores, by catalyst-free two-step SiH_4 chemical vapor deposition, where the metallic core acts as a mechanical supporter and a kinetically unlimited charge supplier. We have achieved highly reversible capacitance of over 3000 mAh g^{-1} even at a 2C rate, with stable cyclic retention which stems from the altered electrochemical reactions with relatively small volume expansion routes by a kinetic effect.

Introduction

Anode architectures, particularly when they are three-dimensional at the nanometre scale, are closely related with cell performances in Li-ion batteries.[1–6] Therein, the achievable electrochemical capacity and the power characteristics are inherently determined by a series of phase transitions involved in the anode during lithiation/delithiation. The electrochemical Li–Si system forms various Li-rich Li$_x$Si intermetallics ($0 \leq x \leq 4.4$), correspondingly symptomatic of the largest known gravimetric charge capacity of up to 4200 mAh g^{-1} in the bulk limit, thus can represent an attractive anodic system for the high capacity Li-ion battery.[1,3–5]

However, the system undergoes notoriously large volume-changes up to 400% during the cyclic lithiation and delithiation, resulting in poor cyclic retention in its cell capacity and output power.[1,3–5] It is suggested that this severe anode pulverization upon the cyclic volume changes can be alleviated by adopting one-dimensional Si nanocrystals, such as Si nanowires (NWs), based on the promises of their affordable accommodation of large volume-changes and the efficient charge collection capability.[4,5,7–11] Yet, monolithic single-crystalline Si NWs exhibit cyclic degradation in their cell capacity particularly at the high charging/discharging rate, thus limiting their integration into the high power cells.[5,12–18]

Here, we report amorphous-Si (*a*-Si) shell anodes, supported by NiSi$_x$ NW cores, by a catalyst-free two-step SiH_4 chemical vapor deposition, where the metallic core acts as a mechanical supporter and a kinetically unlimited charge supplier. Spontaneous silicide NWs, such as NiSi$_x$, FeSi, CoSi, $TaSi_2$[19–27] NWs, have been recently investigated, and among others NiSi$_x$ NWs are of particular interest because their growth can be easily integrated with silicon processing technology. Besides, NiSi$_x$ exhibits the lowest resistivity and makes good contacts with Si.[25–27] In this regard, we designed the core-shell NW anode architecture in this work. We have achieved the highly reversible capacity over 3000 mAh g^{-1} even at 2C rate, with stable cyclic retention which stems from the altered electrochemical reactions with relatively small volume expansion routes by a kinetic effect.

Results and discussion

a-Si NW shells, supported by metallic NiSi$_x$ NW cores (*a*-Si/NiSi$_x$ NW), were grown by a simple two-step SiH_4 CVD process: (i) the self-catalytic NiSi$_x$ NWs were grown on Ni thin films, (ii) followed by *a*-Si shells deposition on the NiSi$_x$ NWs, as illustrated in Fig. 1(a). We start off the NiSi$_x$ NW synthesis by thermal evaporation of Ni films on Ag-coated stainless steel (SUS) substrates of a circular shape disk in 15mm diameter. Ag acts as a diffusion barrier of Fe from SUS into the Ni films. The Ni/Ag/SUS substrates were annealed with oxygen at 400 °C, and then reacted with 50 Torr of SiH_4 (10% diluted in H_2) at 420 °C, as described in Ref. 26,27. The *a*-Si shell deposition was conducted by using thermal decomposition of SiH_4 (10% diluted in H_2) at 550 °C for 30 min. Here we note that *a*-Si shells are formed, when NiSi$_x$ NWs are oxygen-exposed prior to the SiH_4 flows, whereas the crystalline Si shell (*c*-Si) was formed otherwise, as shown in Fig. S1.† We also prepared *a*-Si shell NWs on the insulating *c*-Si core NWs, and describe a series of

[a]*Department of Materials Science and Engineering, Pohang University of Science and Technology (POSTECH), San 31, Hyoja-Dong, Nam Gu, Pohang, Gyungbuk, 790-784, Korea. E-mail: mhjo@postech.ac.kr; Fax: +82-54-279-2399; Tel: +82-54-279-2158*
[b]*Division of Advanced Materials Science, Pohang University of Science and Technology (POSTECH), San 31, Hyoja-Dong, Nam Gu, Pohang, Gyungbuk, 790-784, Korea*
[c]*Division of Advanced Materials Engineering, Kongju National University, 275 Budae-Dong, Cheonan, Chungnam, 330-717, Korea. E-mail: dake1234@kongju.ac.kr; Tel: +82-41-521-9378*

† Electronic supplementary information (ESI) available: Structure of *c*-Si/NiSi$_x$ NW, a photograph of the *a*-Si/NiSi$_x$ NW grown on substrate, normalization method for calculating the gravimetric capacity, and current charge/discharge curve for NiSi$_x$ NW cell in the galvanostatic mode. See DOI: 10.1039/c0sc00628a

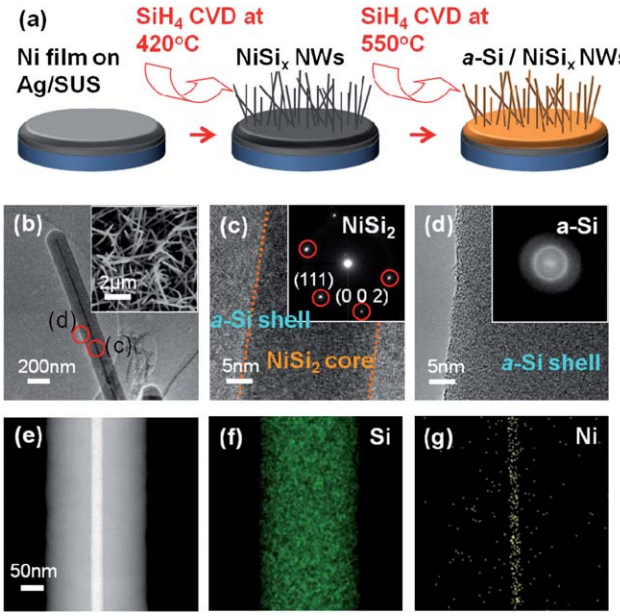

Fig. 1 (*In color*) (a) The schematics of the NW heterostructure growth in this study. (b) TEM image of an individual *a*-Si/$NiSi_x$ NW. The inset shows a plan-view SEM image of *a*-Si /$NiSi_x$ NWs grown on SUS substrate. (c) HRTEM image of an individual *a*-Si/$NiSi_x$ NW at the core region and the corresponding FFT-DP along the [1–10] zone axis (inset). (d) HRTEM image of an individual *a*-Si/$NiSi_x$ NW at the shell region and the corresponding FFT-DP (inset). (e) HAADF image of *a*-Si/$NiSi_x$ NW. (f and g) EDX elemental mapping images of Si (f) and Ni (g) in (e).

comparative cyclic cell performances in greater details,[28] and discuss them around the roles of the metallic core for altered electrochemical reactions.[29,30]

Fig. 1(b) shows the representative microstructures of *a*-Si/$NiSi_x$ NWs by transmission electron microscope (TEM), where the average diameter of *a*-Si/$NiSi_x$ NW is 190 nm with the 20 nm thick $NiSi_x$ core NWs. Scanning electron microscope (SEM) images in the inset illustrate that the shell NWs were conformally deposited onto the whole NWs in the substrate – see also Fig. S2 in Supporting Information.† High-resolution TEM (HRTEM) images and corresponding fast fourier transform diffraction patterns (FFT-DP) in Fig. 1(c) and 1(d) confirm that Si/$NiSi_x$ NW features amorphous Si NW shells and single-crystalline $NiSi_2$ NW cores.[31] High-angle annular dark field (HAADF) images, where the intensity is roughly proportional to square of atomic number, and energy dispersive X-ray spectroscopy (EDX) mapping images in Fig. 1(e), (f) and (g) also demonstrate that core/shell NW structures are clearly discernable, and the elemental distribution of Ni is locally limited in the core region within the instrumental resolution.

The *a*-Si/$NiSi_x$ NW anodes were incorporated into a coin-type half cell (CR2016 coin-type). The cell uses Li metal foils as the counter and the reference electrode, and 1M $LiPF_6$ dissolved in a 1 : 1 (by volume, provided by Techono. Semichem. Co.) mixture of ethylene carbonate (EC) and diethyl carbonate (DEC) as the electrolyte. The cell assembly was carried out in an Ar-filled glove box with less than 0.1 ppm each of oxygen and moisture. The charge capacity of the *a*-Si/$NiSi_x$ NW cell was measured over the potential range of 0.01 to 2.00 V (*vs.* Li/Li^+) during the initial 50 cycles in the galvanostatic mode. The measured discharge capacity is carefully normalized into the gravimetric capacity, as described in Fig. S3.†

Fig. 2 shows the cyclic retention of two types of NWs: *a*-Si/$NiSi_x$ NW cells and *a*-Si/*c*-Si NW cells. It is found that *a*-Si/$NiSi_x$ NWs retain almost the 83% of the first discharge capacity after the 50th cycle with the high charge capacity above 3000 mAh g^{-1}. For a check, we tested the bare $NiSi_x$ NW anodes in the galvanostatic mode; however, we did not observe any apparent potential plateau over the potential range of 0.01 to 3.00 V – also see Fig. S4.† This suggests that the bare $NiSi_x$ NWs alone are electrochemically inactive in our experimental conditions. We have also tested the rate dependent capacity by charging the cell at a constant rate of 0.1C and discharging it at the various rate from 0.1C to 2C (1C≡1 h per half-cycle). Fig. 2(b) shows that the discharge capacity of *a*-Si/$NiSi_x$ NWs is maintained over 94% of the first discharge capacity, and weakly depends on the C-rate up to 2C. The discharge capacity of *a*-Si/*c*-Si NWs, on the other hand, fades significantly and strongly depends on the C-rate. It is obvious that a combination of *a*-Si shells and metallic $NiSi_x$ NW cores is responsible for the unprecedented reversible lithiation/delithiation in *a*-Si shells at the high charge/discharge rate.

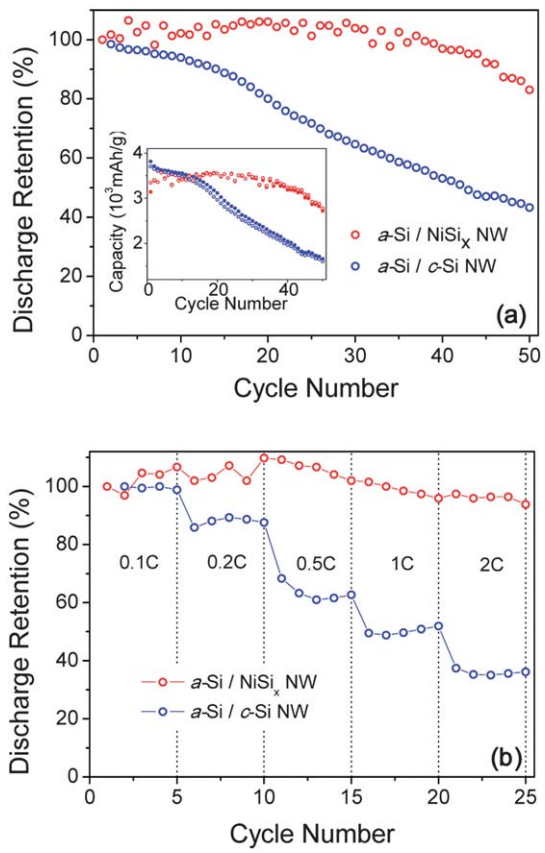

Fig. 2 (*In color*) (a) The discharge capacity retention for the *a*-Si/$NiSi_x$ NW (red circles) and the *a*-Si/*c*-Si NW (blue circles), respectively. The inset shows the specific capacity for the *a*-Si/$NiSi_x$ NW (red close circles-charge and red open circles-discharge) and the *a*-Si/*c*-Si NW (blue close circles-charge and blue open circles-discharge), respectively. (b) The rate capability for the *a*-Si/$NiSi_x$ NW (red circles) and the *a*-Si/*c*-Si NW (blue circles), respectively.

Fig. 3(a–c) present HRTEM and HAADF images of *a*-Si/*c*-Si NWs after the 50 cycles, where they become porous and pulverized upon the cyclic lithiation/delithiation. By striking contrast, *a*-Si/NiSi$_x$ NWs maintain the initial core/shell NW structures. Apparently, the structural robustness in *a*-Si/NiSi$_x$ NWs, guaranteed from a mechanical supporter of NiSi$_x$ cores, is responsible for the enhanced cyclic retention and rate capability, as shown in Fig. 3(d–f).

In order to further investigate the electrochemical roles of the metallic NiSi$_x$ cores, we tried to compare the differential capacity plots for *a*-Si/NiSi$_x$ NWs with those of *a*-Si/*c*-Si NWs, as in Fig. 3 (g). After the 1st cycle, which is called the formation or activation process, *a*-Si/*c*-Si NWs and *a*-Si/NiSi$_x$ NWs display two reduction peaks around 260 mV and 80 mV, as marked by *A* and *B*, and they are associated with the formations of intermetallic compounds, Li$_x$Si. Reportedly, the 260 mV and 80 mV peaks are assigned to the formation of amorphous Li$_x$Si (*a*-Li$_x$Si) from *a*-Si and *c*-Si, respectively.[32–34] Although other small reduction peaks below 80 mV, marked as *C* and *C*′, are not well identified, they are usually assigned to either routes for *a*-Li$_x$Si to *a*-Li$_{x+y}$Si (fully lithiated amorphous lithium silicides) transition or *a*-Li$_x$Si to *c*-Li$_z$Si (fully lithiated crystalline lithium silicides) transition.

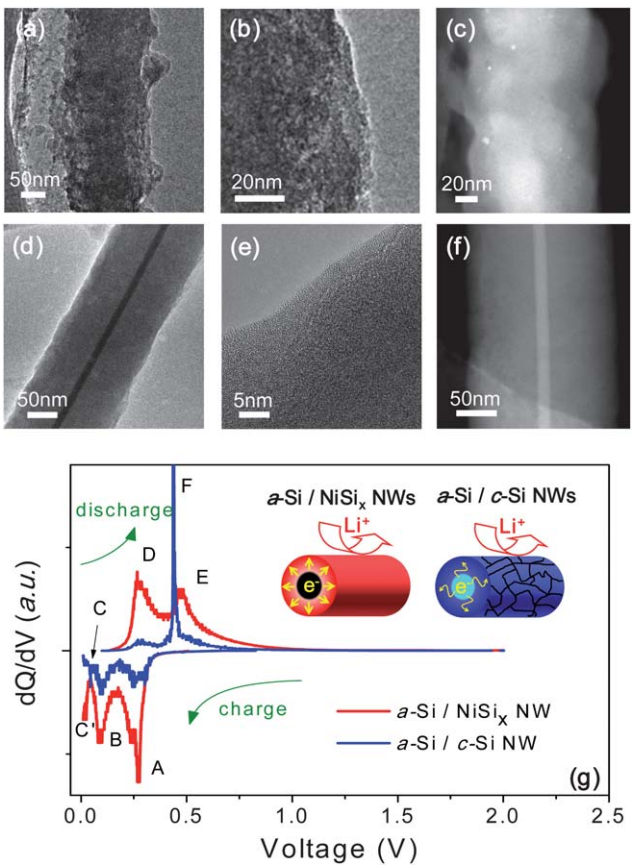

Fig. 3 (*In color*) (a–f) TEM images of individual *a*-Si/*c*-Si NW and *a*-Si/NiSi$_x$ NW after 50th cycling. (a) Low magnitude TEM image of *a*-Si/*c*-Si NW. (b) HRTEM image of *a*-Si/*c*-Si NW at the surface. (c) HAADF image of *a*-Si/*c*-Si NW. (d) Low magnitude TEM image of *a*-Si/NiSi$_x$ NW. (e) HRTEM image of *a*-Si/NiSi$_x$ NW at the surface. (f) HAADF image of *a*-Si/NiSi$_x$ NW. (g) The differential capacity of the 10th cycle for the *a*-Si/NiSi$_x$ NW (red line), the *a*-Si/*c*-Si NW (blue line).

Identification of the fully lithiated phase whether it is *a*-Li$_x$Si to *c*-Li$_z$Si is critical, since the *a*-Li$_x$Si to *c*-Li$_z$Si or *vice versa* among the series of lithiation/delithiation reactions involves the largest volume changes, which is in turn the major source for the deterioration in the anodic reversibility.[34–37] During the discharge process, *a*-Si/*c*-Si NWs display the dominant oxidation peak at 450 mV, marked as *F*, assigned to the dissociation of *c*-Li$_z$Si to *a*-Li$_x$Si or *a*-Si, indicating that its reduction peak below 80 mV corresponds to the nucleation of a crystalline lithium silicide (*c*-Li$_z$Si).[34–36] By contrast, *a*-Si/NiSi$_x$ NWs exhibit two dissimilar oxidation peaks between 250 mV and 500 mV, marked as *D* and *E*, which are assigned to the dissociation of *a*-Li$_{x+y}$Si to *a*-Li$_x$Si or *a*-Si.[32,34,37] This finding can be back-traced to assign another phase transition, *C*′ during the Li charging to the formation of *a*-Li$_{x+y}$Si. In other words, the full lithiation into *a*-Li$_{x+y}$Si in *a*-Si/NiSi$_x$, instead of *c*-Li$_z$Si in *a*-Si/*c*-Si NWs, alleviates severe physical pulverization and leads to the stable reversibility in the cyclic cell performance. We speculate that kinetically unlimited electron supply from NiSi$_x$ NW core coupled with the properly absorbed volume change by *a*-Si shell provides alternative electrochemical reactions of *a*-Si/NiSi$_x$ NWs to skip over the nucleation of *c*-Li$_x$Si by a kinetic effect. We measured average resistivity of NiSi$_x$ NWs and *c*-Si NWs to be 10^{-3} Ω·cm, and 10^{3} Ω·cm. It is known that monolithic Si crystals usually undertake temporal local-concentration of Li ions in Si matrices, followed by the rapid and spatially inhomogeneous evolution of fully lithiated crystalline lithium silicides (*c*-Li$_z$Si), which in turn results in severe Si pulverizations. Instead, we argue that uniform distribution of the electrochemical potential in our *a*-Si/NiSi$_x$ NWs, which is provided by the metallic NiSi$_x$ cores is responsible for the reversible reaction route mediated by fully lithiated amorphous lithium silicides.[3,32,36]

Acknowledgements

M.-H.J. acknowledges the support from the Nano Original & Fundamental Technology R&D Program (2010-0019195), the Priority Research Centers Program (2010-0029711), the Basic Research Program (2010-0001873 and 2010-0017853), the Mid-career Researcher Program (2010-0027627) and the WCU Program (R31-2008-000-10059-0) through the National Research Foundation (NRF) of Korea funded by the Ministry of Education, Science, and Technology (MEST), and POSCO. Y.-M.K. acknowledges the Converging Research Center Program (2010K001097) and the Basic Science Research Program (20090072972) through the NRF of Korea funded by the MEST.

Notes and references

1 P. G. Bruce, B. Scrosati and J.-M. Tarascon, *Angew. Chem., Int. Ed.*, 2008, **47**, 2930.
2 I. Grigoriants, L. Sominski, H. Li, I. Ifrgan, D. Aurbach and A. Gedanken, *Chem. Commun.*, 2005, **7**, 921.
3 S.-H. Ng, J. Wang, D. Wexler, K. Konstantinov, Z.-P. Guo and H.-K. Liu, *Angew. Chem., Int. Ed.*, 2006, **45**, 6896.
4 H. Kim and J. Cho, *Nano Lett.*, 2008, **8**, 3688.
5 J. R. Szczech and S. Jin, *Energy Environ. Sci.*, 2011, **4**, 56.
6 J. R. Dahn, T. Zheng, Y. Liu and J. S. Xue, *Science*, 1995, **270**, 590.
7 C. K. Chan, H. Peng, G. Liu, K. Mcilwrath, X. F. Zhang, R. A. Huggins and Y. Cui, *Nat. Nanotechnol.*, 2008, **3**, 31.

8 K. Peng, J. Jie, W. Zhang and S.-T. Lee, *Appl. Phys. Lett.*, 2008, **93**, 033105.
9 H. Kim, B. Han, J. Choo and J. Cho, *Angew. Chem., Int. Ed.*, 2008, **47**, 10151.
10 J. Graetz, C. C. Ahn, R. Yazami and B. Fultz, *Electrochem. Solid-State Lett.*, 2003, **6**, A194.
11 C. K. Chan, X. F. Zhang and Y. Cui, *Nano Lett.*, 2008, **8**, 307.
12 A. Magasinski, P. Dixon, B. Hertzberg, A. Kvit, J. Ayala and G. Yushin, *Nat. Mater.*, 2010, **9**, 353.
13 B. Gao, S. Sinha, L. Fleming and O. Zhou, *Adv. Mater.*, 2001, **13**, 816.
14 L.-F. Cui, Y. Yang, C.-M. Hsu and Y. Cui, *Nano Lett.*, 2009, **9**, 3370.
15 S. Zhou, X. Liu and D. Wang, *Nano Lett.*, 2010, **10**, 860.
16 L.-F. Cui, R. Ruffo, C. K. Chan, H. Peng and Y. Cui, *Nano Lett.*, 2009, **9**, 491.
17 S. Zhang, Z. Du, R. Lin, T. Jiang, G. Liu, X. Wu and D. Weng, *Adv. Mater.*, 2010, **22**, 5378.
18 T. Song, J. Xia, J.-H. Lee, D. H. Lee, M.-S. Kwon, J.-M. Choi, J. Wu, S. K. Doo, H. Chang, W. I. Park, D. S. Zang, H. Kim, Y. Huang, K.-C. Hwang, J. A. Rogers and U. Paik, *Nano Lett.*, 2010, **10**, 1710.
19 A. L. Schmitt, M. J. Higgins, J. R. Szczech and S. Jin, *J. Mater. Chem.*, 2010, **20**, 223.
20 J. R. Szczech and S. Jin, *J. Mater. Chem.*, 2010, **20**, 1375.
21 A. L. Schmitt, M. J. Higgins, D. Schmeisser, F. J. Himpsel and S. Jin, *Nano Lett.*, 2006, **6**, 1617.
22 Y. Song, A. L. Schmitt and S. Jin, *Nano Lett.*, 2006, **6**, 965.
23 K. Seo, K. S. K. Varadwaj, P. Monhanty, S. Lee, Y. Jo, M.-H. Jung, J. Kim and B. Kim, *Nano. Lett.*, 1240, **2007**, 7.
24 Y.-L. Chueh, M.-T. Ko, L.-J. Chou, L.-J. Chen, C.-S. Wu and C.-D. Chen 2006, 6, p. 1637.
25 K. Kang, C.-J. Kim and M.-H. Jo, *J. Appl. Phys.*, 2009, **105**, 122407.
26 K. Kang, S.-K. Kim, C.-J. Kim and M.-H. Jo, *Nano Lett.*, 2008, **8**, 431.
27 C.-J. Kim, K. Kang, Y. S. Woo, K.-G. Ryu, H. Moon, J.-M. Kim, D.-S. Zang and M.-H. Jo, *Adv. Mater.*, 2007, **19**, 3637.
28 K. Kang, H.-S. Lee, D.-W. Han, G.-S. Kim, D.-H. Lee, G. Lee, Y.-M. Kang and M.-H. Jo, *Appl. Phys. Lett.*, 2010, **96**, 053110.
29 J. Yin, M. Wada, K. Yamamoto, Y. Kitano, S. Tanase and T. J. Sakai, *J. Electrochem. Soc.*, 2006, **153**, A472.
30 Graetz, C. C. Ahn, R. Yazami and B. Fultz, *Electrochem. Solid-State Lett.*, 2003, **6**, A194.
31 Crystal structure of Si: diamond cubic, lattice constant: 5.431 Å, space group: Fm3m, JCPDS 43–0989; Crystal structure of $NiSi_2$: diamond cubic, lattice constant: 5.416 Å space group: Fd-3m, JCPDS 27–1402.
32 M. N. Obrovac and L. J. Krause, *J. Electrochem. Soc.*, 2007, **154**, A103.
33 J. P. Maranchi, A. F. Hepp and P. N. Kumta, *Electrochem. Solid-State Lett.*, 2003, **6**, A198.
34 C. K. Chan, R. Ruffo, S. S. Hong, R. A. Huggins and Y. Cui, *J. Power Sources*, 2009, **189**, 34.
35 T. D. Hatchard and J. R. Dahn, *J. Electrochem. Soc.*, 2004, **151**, A838.
36 Y. M. Kang, S. M. Lee, S. J. Kim, G. J. Jeong, M. S. Sung, W. U. Choi and S. S. Kim, *Electrochem. Commun.*, 2007, **9**, 959.
37 N. Obrovac and L. Christensen, *Electrochem. Solid-State Lett.*, 2004, **7**, A93.